Numerical modeling of the effects of impact conditions, foundation stiffness, and cable pretension on the behavior of high-tension guard cable systems

Juan P. Giraldo-Isaza [a], Oliver Giraldo-Londoño [a,*], Glenn A. Washer [a], John J. Myers [b]

[a] Department of Civil and Environmental Engineering, University of Missouri, W1024 Lafferre Hall, Columbia, MO 65211, USA
[b] Civil, Architectural and Environmental Engineering, Missouri University of Science and Technology, Butler-Carlton Hall, 1401 N. Pine Street, Rolla, MO 65409, USA

ARTICLE INFO

ABSTRACT

Cable barriers are one type of road restraint system commonly used on highways across the United States to contain and redirect errant vehicles and to prevent crossover accidents. These systems are typically tested under the provisions from safety manuals considering standard crash conditions (e.g., vehicle speed and impact angle). To understand the performance of cable barriers, it is important to evaluate the effects of non-standard crash and system conditions, including various vehicle speeds, impact angles, foundation material stiffness, and cable pretension loads. For that purpose, we created a set of full-scale finite element models in LS-DYNA to assess the effects of these non-standard conditions on the performance of high-tension cable barrier systems. The results from the models show that soft soils and under-tensioned systems yield higher cable deflections. Moreover, the results indicate that speeding vehicles colliding at non-standard angles increase cable tensions by up to 91% and cable deflections by up to 318%. These findings highlight the importance of evaluating cable barrier performance under more severe scenarios, which could lead to system failure and more severe collision consequences.

1. Introduction

According to the AAA Foundation for Traffic Safety [1], half of American drivers reported driving 25 km/h over the speed limit on the freeway in 2021, which is concerning, given that speeding is a significant factor in fatal crashes. To help mitigate the risk of occupant injuries or fatalities, state agencies have made significant investments in road safety equipment such as guard cable systems. However, how these systems perform when impacted by speeding vehicles at non-standard angles or under various soil and pretension conditions is still being determined. Answering this critical question could help to improve the safety of our roadways.

Fig. 1 shows one of the typical cable barrier systems found in the United States. These cable systems are a type of roadside safety barrier designed to contain and redirect errant vehicles and are typically composed of a series of cables mounted on posts. Despite their popularity, cable barriers have yet to be extensively tested (i.e., considering non-standard crash conditions). As a result, local authorities rely on manufacturer guidelines and recommendations to evaluate their effectiveness in containing and redirecting

---

* Corresponding author.
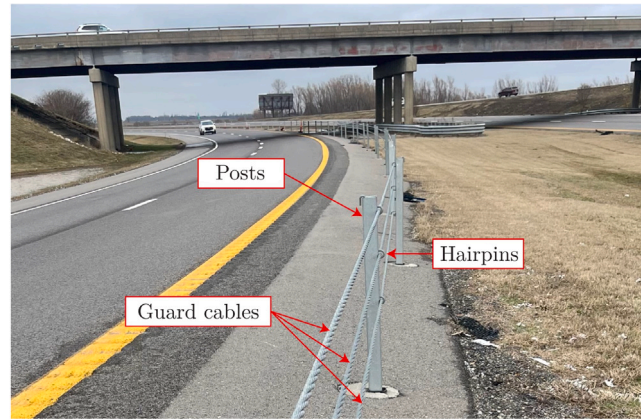 E-mail address: ogiraldo@missouri.edu (O. Giraldo-Londoño).

Fig. 1. Typical high-tension guard cable system found in the United States. The road safety system is composed of three guard cables supported and held in position by a set of steel posts and hairpins.

vehicles impacting at standard crash conditions.[1] Furthermore, due to the high cost of performing full-scale physical tests, limited data is available regarding how factors such as vehicle speed, cable pretension, impact angle, or foundation material stiffness affect the performance of these systems.

In recent years, numerical models have been developed to overcome the constraints associated with full-scale testing of vehicle impacts, producing accurate representations of impact scenarios at a fraction of the cost. The present study aims to develop a set of full-scale finite element models in LS-DYNA to investigate the performance of typical high-tension cable barriers when impacted by a 900-kg Chevrolet Geo Metro under different crash conditions. Parameters such as vehicle speed, impact angle, foundation material stiffness, and cable pretension are varied to assess their influence on the global performance of the cable barrier system.

Manufacturers test guard cable barriers to comply with safety standards such as the National Cooperative Highway Research Program (NCHRP) Report No. 350 [2]. In this document, a vehicle speed of 100 km/h and an impact angle of 20° are recommended for vehicles with a mass of 820 kg (820C). However, our simulations revealed that vehicles traveling at higher speeds, such as 115 or 130 km/h, and impacting at angles of 30° or 40° could produce up to 91% higher cable tensions than those obtained at standard conditions, exacerbating the risk of cable failure. Moreover, vehicles impacting under-tensioned systems or with softer foundation materials can displace more considerable lateral distances, amplifying the risk of cars striking roadside obstacles. The findings of this study provide valuable insights into the safety of cable barriers under real-world conditions and inform the design and deployment of these systems.

The remainder of this paper is organized as follows. Section 2 summarizes relevant studies in the literature dealing with the numerical modeling of guard cable systems and their components. Next, Section 3 discusses our numerical model and its implementation in LS-DYNA. In Section 4, we calibrate our model by comparing our numerical results against experimental results obtained from full-scale crash tests. In Section 5, we use the model to understand the system behavior under non-standard crash and system conditions such as higher speeds, impact angles, foundation material stiffness, and cable pretension loads. Then, we finalize the paper with some concluding remarks in Section 6.

2. Background

Computer simulations are powerful and rapidly developing tools that have enabled researchers to study the behavior of cable barrier systems [3]. Multiple researchers have used computer simulations to study road safety devices [3–14]. Some studies have focused on the numerical modeling of system components [6,11,15,16], whereas others have considered full-scale numerical models of guard cable systems under standard and non-standard impact conditions [3–5,17–19].

2.1. Standard crash conditions

Mohan et al. [4] used LS-DYNA to simulate the impact of a 2000 kg Chevrolet pickup truck on a three-strand cable barrier system as per the conditions outlined in the NCHRP Report 350 [2]. They validated their model by comparing it with full-scale crash tests and found a strong correlation between vehicle and cable behavior. Building upon this work, Marzougui et al. [5] investigated low-tension, three-strand cable barriers on sloped terrains. Their study revealed that sloped terrains may lead to underrides and median crossovers and that barriers located over 0.3 m from the median center may not effectively protect smaller vehicles. Both studies adhered to the NCHRP 350 impact conditions regarding impact angle and vehicle speed.

---

[1] Standard crash conditions correspond to a 20° impact angle and a 100 km/h vehicle speed per the National Cooperative Highway Research Program Report 350 recommended values for the 820C test vehicle [2].

Recently, Bruski et al. [20] conducted a study on the performance of curved high-tension cable barriers with anti-glare screens following the EN 1317 standard [21,22]. Although the barriers were found to work properly, the authors emphasized that crash tests defined in the EN 1317 standard do not cover the entire range of accidents that might happen on roads. Therefore, continuous research on the performance of road safety barriers under various impact conditions is necessary.

2.2. Non-standard crash conditions

The performance of cable barrier systems is influenced by various factors, including impact conditions (such as vehicle speed, impact angle, and mass), barrier design, and environmental conditions [23]. Consequently, it is challenging to accurately predict system performance based solely on tests conducted under standard impact conditions. To address this limitation, recent studies have investigated the performance of cable barriers under a wider range of crash scenarios, revealing significant deviations from standard crashworthiness criteria.

Bruski and Witkowski [18] investigated the effects of barrier height, cable tension, impact angle, and impact speed, and found that a 5 cm increase in barrier height can increase maximum cable deflections by 27%, raising the risk of hitting obstacles such as road lamps. They also found that under-tensioned systems increase vehicle-barrier contact length and that a higher impact angle significantly increases cable lateral deflections. Subsequent work by Bruski et al. [3,10] highlighted the importance of evaluating cable barriers under varying conditions, showing that non-standard impact angles can lead to vehicle rollovers and that soil degradation may result in increased barrier damage. Additionally, Fang et al. [17] demonstrated that cable height, vehicle speed, and impact angle significantly influence barrier performance, with large angles and high speeds increasing impact severity and risk of collisions. Further addressing the challenge of high-speed impacts, Kee-Dong Kim et al. [24] developed new semi-rigid cable barriers able to resist small car impacts with speeds higher than 160 km/h. These studies collectively highlight the critical need to consider non-standard conditions in crash modeling to ensure the effectiveness and safety of cable barriers.

2.3. Modeling of guard cable components

Guard cable systems typically consist of three cables attached to evenly spaced posts using hairpins and lock plates, as depicted in Fig. 1. To ensure an accurate representation of the physical system, it is essential to incorporate each component into the numerical model. Additionally, appropriate contact algorithms should be utilized to model the interaction between each part. Addressing the four primary element interaction simulation challenges outlined in [5] is crucial, including the interaction between (i) post-hook and bolt, (ii) soil and post, (iii) cable and hook, and (iv) cable and vehicle. In the following subsections, we will explore the modeling approaches employed to simulate each component of cable barriers and highlight the most commonly used LS-DYNA keywords for defining section properties, material properties, and contact definitions.

2.3.1. Wire rope modeling

Modeling guard cables is challenging due to the nonlinear behavior of the wire ropes, which involves significant deformations and plasticity. Advanced material laws and contact algorithms are necessary to overcome this challenge, along with element formulations that reduce the number of degrees of freedom in the model [25]. Depending on the specific application, one can use various methods to model wire ropes in LS-DYNA, including beam, shell, and solid elements. Beam elements are typically used to represent the global behavior of a cable barrier, while shell elements are used to model the local behavior of a cable [7,8,16]. For example, Mohan et al. [4] and Marzougui et al. [5] used discrete beam elements to model three-strand cable barriers, which are simple to use and quick to implement. However, these elements cannot fully capture the cable complex behavior, especially the bending or torsional stiffness of wires, which can result in inaccurate results [26]. Despite these limitations, the modeling methodology used by Mohan et al. [4] and Marzougui et al. [5] produced results that closely matched those from physical tests.

Later, Stolle and Reid [7] addressed the limitations of discrete beam elements by developing an improved finite element model for 19-mm diameter 3×7 wire ropes commonly used in roadside cable barrier systems using the material property curves displayed in Fig. 2a–c. Their improved wire model combines the Belytschko–Schwer beam formulation and the moment–curvature beam material model from LS-DYNA and ANSYS [26]. This formulation allowed them to capture not only the mechanical properties of the cable but also the correct contact behavior through a virtual contact surface, such as the one shown in Fig. 2e.

The Belytschko–Schwer beam formulation can achieve fairly accurate reaction forces and moments without requiring precise cross-sectional definitions, which avoids using solid elements at an increased computational cost. This beam formulation incrementally solves the dynamic equations for acceleration, forces, and moments to subsequently obtain the moment–curvature beam material model, element axial strains, curvatures, and axial unit twist. This process circumvents the calculation step of section stresses and strains required by other modeling techniques, such as solid formulations. In a related study, Stolle and Reid [7] found that the Belytschko–Schwer beam provides a good comparison with rope reactions in full-scale experimental tests, allowing different researchers to adapt that beam formulation successfully into their finite element models [3,18].

Table 1 presents the typical section and material parameters used in LS-DYNA to simulate cables using Belytschko–Schwer beam elements coupled with the moment–curvature beam material model. The parameter values are retrieved from the report by Reid et al. [27] whose cable model has been implemented by numerous researchers in their guard cable simulations [3,8,18].

In this work, we implemented the model corresponding to prestreched cables using the simplifications recommended by Reid et al. [27]. In their report, they simplified the cable area as a full 19 mm diameter circle to enhance the contact behavior of the model, as shown in Fig. 2e. However, this modeling approach requires to scale the density and the Young Modulus from a value
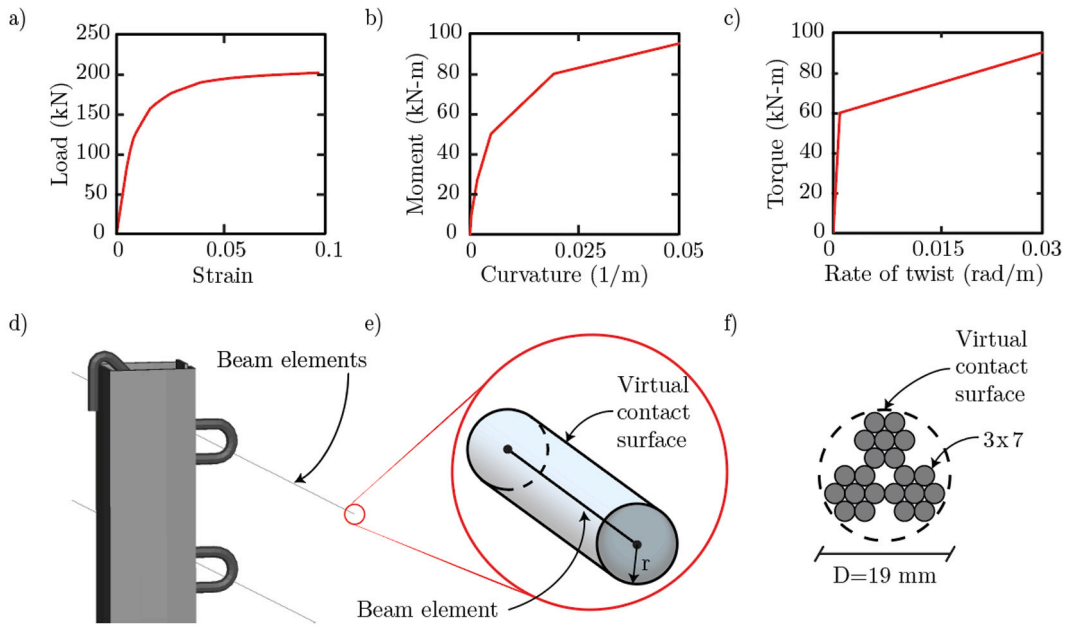
Fig. 2. Mechanical behavior of the cables (top) and description of the simplified cable model (bottom): (a) load vs. strain relationship; (b) moment vs. curvature relationship; (c) torque vs. rate of twist relationship (adopted from [7]); (d) general beam setup; (e) virtual contact surface; and (f) physical meaning of the virtual contact surface.

Table 1
Section properties for the cable model.

Variable	Description	Value[a]
ELFORM	Element formulation	2
SHRF	Shear factor	0.9
QR/IRID	Quadrature rule	2
CST	Shear factor	1
A	Cross-sectional area mm^2	285.02
ISS	Area moment of inertia about local s-axis mm^4	6464.72
ITT	Area moment of inertia about local t-axis mm^4	6464.72
RO	Mass density (kg/m^3)	4308.5
E	Young's modulus (GPa)	62.88

[a] Values retrieved from the report by Reid et al. [27].

of 7948 kg/m^3 and 116 GPa, to 4308.5 kg/m^3 and 62.88 GPa, respectively.[2] Hence, we implemented the corresponding modified material properties in the present work.

2.3.2. Soil modeling

Three main approaches are typically employed to study the interaction between cable barrier posts and the supporting soil during dynamic loading. The first approach uses solid elements with the material keyword `MAT_FHWA_SOIL` [28,29]. This material keyword requires tuning 24 individual parameters, including density, specific gravity, water density in the material, Drucker–Prager parameter, bulk modulus, void deformation energy, and viscoplasticity parameters 1 and 2 [30]. The second approach, developed by researchers at NASA for dynamic impact simulations, uses solid elements with the material keyword `MAT_005_SOIL_AND_FOAM` [6]. This material model requires tuning only six individual parameters, which facilitates its implementation in models where the exact soil properties are unknown. Its simplicity and ease of implementation explain its popularity among recent studies on roadside barriers [3,10,18,25,31]. Moreover, subsequent studies have contributed to the generality of the model. For instance, Klasztorny et al. [11] used the model from [6] and included an algorithm to obtain a set of elastoplastic parameters for soft, medium, and hard plastic cohesive soils. These parameters were later used by Baranowski and Damaziak [19] in a parametric study on the influence of soil stiffness in vehicle-lighting pole crash tests.

Despite the virtues of these models, using solid elements for soil simulation can be computationally expensive, especially for full-scale finite element models of guard cable systems. To address this limitation, a third approach proposed by Hiser and Reid

---

[2] The density and the Young's modulus are scaled using the ratio of the real cross-sectional area (154.5 mm^2) to the modeled cross-sectional area (285.02 mm^2). This operation aims to preserve the linear density of the cable and maintain the original time step.
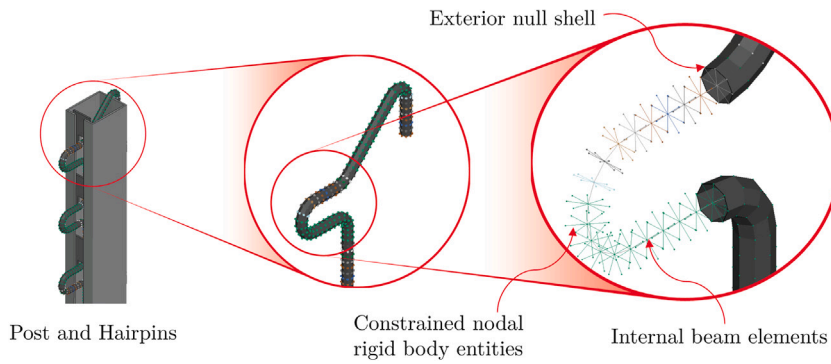
Fig. 3. Illustration of the hairpin modeling approach, where beam elements are enveloped in null shells, kinematically constrained to the beam nodes for precise contact modeling.

[15] employed a simplified soil model using discrete spring elements with linear elastic properties, which heavily improves the computational efficiency as no additional degrees of freedom are introduced into the model. As discussed later, our work employs a combination of a high-fidelity solid soil model near the impact location and a simplified soil model using spring elements away from the impact location. This choice aims to reduce the computational cost while maintaining model fidelity near the impact location.

2.3.3. Post modeling

Posts are typically modeled using 2D shell elements based on the Belytschko–Tsay formulation (ELFORM = 2) [11] combined with a linear plasticity material model. Bruski et al. [3] implemented the `MAT_PIECEWISE_LINEAR_PLASTICITY` material model to account for the elastoplastic properties of steel posts. This is one of the most popular material models in LS-DYNA, as it can account for a wide range of steel behaviors, such as strain hardening and softening. In their model, the authors accounted for strain rate effects using the Cowper and Symonds model [3,26,32].

2.3.4. Hairpin modeling

In guard cable systems, hairpins are used as cable-to-post attachments to secure the cables to the posts. One of the most detailed studies on cable-to-post attachments was published by Stolle et al. [8]. They compared a solid element model and a beam element model of a keyway bolt attachment in cable barriers. While the solid model was more accurate than the beam model, the authors found that a simplified beam representation was desirable for incorporating post attachments into full-scale models in a computationally efficient way. This model wrapped a set of beam elements with null shells, as shown in Fig. 3. Null shells are a type of shell element with no stiffness properties and designed solely to enhance contact modeling. This method prevented numerical instabilities in beam-to-solid contact cases. To avoid excessive deformations of the null shells, their nodes are constrained to the inner beam nodes using `CONSTRAINED_NODAL_RIGID_BODY`. Similar approaches have been used in repository models, such as those created at the National Crash Analysis Center (NCAC) [5] and previous full-scale numerical models of cable barrier systems [3].

2.3.5. Contact modeling

One of the most critical aspects of creating a finite element model of a guard cable system consists of accurately and effectively modeling the contact between components. This involves modeling various interactions such as post-to-soil contact, cable-to-post contact, and vehicle-to-cable contact. Nodal contact modeling with projection-based contact algorithms has been found to be the best approach for simulating interactions between cars and cables, as it eliminates numerical instabilities that arise with other algorithms like `CONTACT_AUTOMATIC_SINGLE_SURFACE` [5]. Additionally, node-based projection can be combined with contacts such as `CONTACT_AUTOMATIC_GENERA1` to eliminate penetration issues and enable successful contact simulations between cars and cables. This approach has been adopted in several studies investigating vehicular collisions against cable barriers [3,8,18].

Additionally, extensions of these algorithms, such as `CONTACT_AUTOMATIC_GENERA1_INTERIOR`, have been used by researchers such as Wilde et al. [25] to model the general contact behavior of system components due to their robustness and ease of implementation. Specific contact applications include hairpin-to-post and post-to-soil contacts. The latter has been implemented using `CONTACT_AUTOMATIC_SURFACE_TO_SURFACE` [3,31]. The typical approach followed by researchers in post-to-soil contacts has been to represent the mass of soil using cylindrical blocks discretized using solid hexahedral elements. Then, the contact with the posts is usually considered indirectly using a closing shell mesh, which is evaluated for contact with the posts in the system using the `CONTACT_AUTOMATIC_SURFACE_TO_SURFACE` contact algorithm. Additionally, some authors have found that using `CONTACT_INTERIOR` in solid soil models can prevent numerical instabilities due to negative volumes [11].
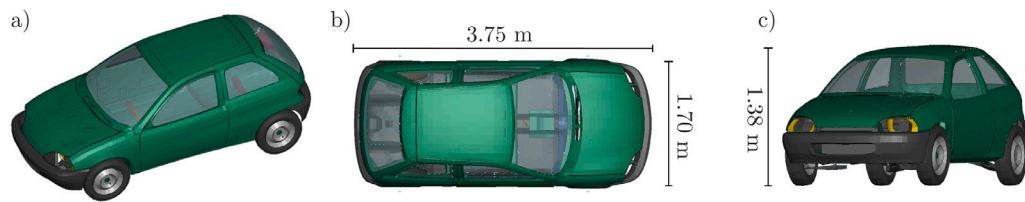
Fig. 4. General view of the Geo Metro numerical model and main vehicle dimensions.

Table 2
General information of the cable barrier model.

Model component	Number of nodes	Number of elements
Cable beams	2365	1181
Post shells	20,731	18,875
Soil solids	33,075	28,896
Soil shells	2208	2112
Soil springs	384	256
Hairpin beams	2565	2584
Hairpin shells	21,014	20,976
Lock plate shells	3192	2204

3. Numerical model

In this section, we discuss the LS-DYNA keywords and parameters used to simulate vehicular impact against a 90-meter-long section of a high-tension cable barrier system. First, we discuss the vehicle model, which was obtained from The National Crash Analysis Center (NCAC) model repository [33] and selected based on the availability of full-scale experimental test results. Next, we elaborate on the finite element model of the three-strand guard cable system and provide details of the cable properties and material parameters associated with the posts, hairpins, and soil models, alongside the element types used for each of these components.

3.1. Vehicle

Some guard cable manufacturers in the United States have conducted studies to evaluate their proprietary cable barrier systems for Test Level 3 conditions using the 900 kg Chevrolet Geo Metro crashing at 100 km/h with an angle of 20°, as per NCHRP 350 [2]. The corresponding LS-DYNA model, shown in Fig. 4, was available in the web archive of The National Crash Analysis Center (NCAC) database [33]. Previous researchers have extensively calibrated this vehicle model [34,35] in numerical simulations of W-beam guardrails and guard cable systems. Therefore, we have selected this vehicle model to conduct our crash simulations and validate the results against the manufacturer experimental results. Interested readers are referred to Bruski et al. [35] for additional information about the validation of this vehicle model for crash simulations.

3.2. Guard cable system

We modeled a typical three-strand high-tension cable barrier system found in the United States (see Fig. 1). Fig. 5 shows a schematic diagram of the cable barrier system. The cable barrier consists of three post-tensioned steel cables (¾-inch 3 × 7), supported by steel C-posts ($8.25 \times 6.35 \times 0.38$-cm thick and 190-cm long) held in place by 1-cm diameter × 60-cm long steel hairpins and lock plates. The hairpins hold the three cables at 50, 63 and 76 cm above ground, respectively. Based on field measurements of typical cable barriers in the United States, the posts are placed on alternate sides of the cables with a 6 m spacing. The total length of the system modeled was 90 m with a length of need of 84 m —the barrier length recommended to adequately shield a roadside obstacle from an errant vehicle that departs a roadway [36]. Excluding the vehicle model, the numerical model of the cable barrier comprises a total of 95,066 nodes and 90,231 elements. A description of the model components is presented in Table 2.

3.2.1. Wire rope

We modeled the wire ropes using the `MAT_MOMENT_CURVATURE_BEAM` material model with Belytschko–Schwer beam elements (ELFORM = 2). The mass density of the cable was set to 4308.5 kg/m³ [3], and the Young's modulus was set to 62.90 GPa. The force-strain, bending moment–curvature, and torque-rate of twist curves shown in Fig. 2 were implemented in the wire rope model based on the properties from [7], which have been successfully used in other studies of guard cable systems [3,10,18,25,31].

We used the `DAMPING_PART_STIFFNESS` and the `DAMPING_FREQUENCY_RANGE` cards to assign damping properties to the cables with a Rayleigh damping coefficient of 0.02 and a fundamental modal damping coefficient of 11% [27] with lower- and upper-frequency bounds of 7 and 70 Hz based on the length proportionality with the values presented in [7].
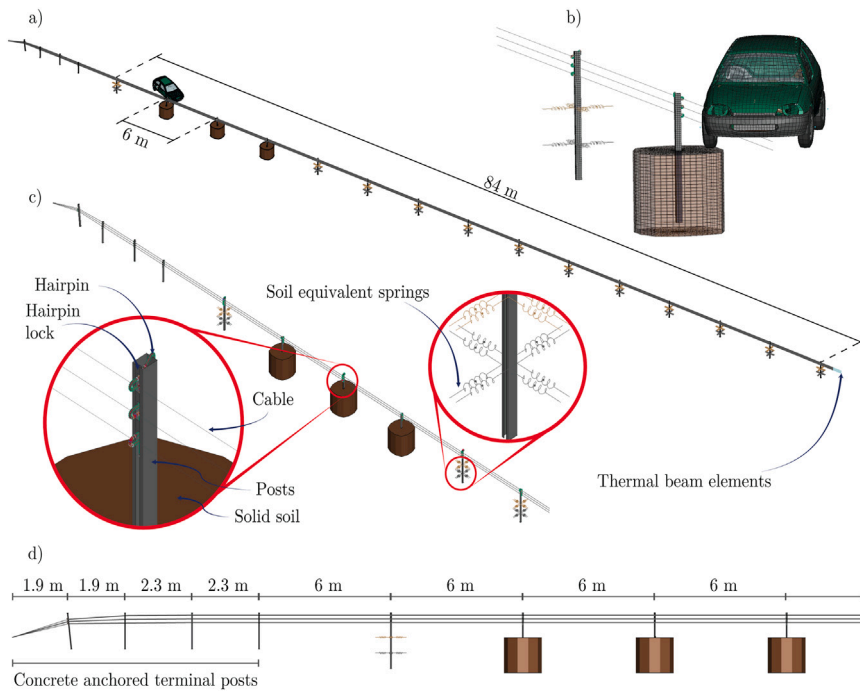
Fig. 5. The views of (a) the total length of the numerical model, (b) the discretization of the finite element model components, (c) the detailed system components, and, (d) a side view with the post spacing.
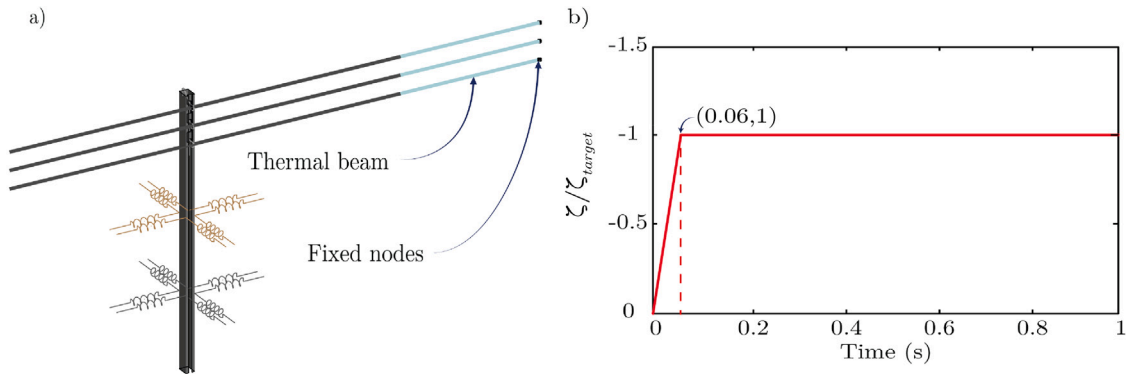

Fig. 6. (a) Thermal elements at downstream edge and boundary conditions (b) Temperature application profile.

Finally, the wire ropes were pretensioned to a target load of 28 kN, as commonly used in American guard cable barriers.[3] The pretension was applied using `ELASTIC_PLASTIC_THERMAL` beam elements at the far end of each cable, as shown in Figs. 5a and 6a. The coefficient of thermal expansion and element length were tuned to achieve the desired cable prestress prior to the impact event. The thermal contraction was achieved by ramping up the cooling temperature, ζ, until reaching the target temperature, ζ_{target}, at 0.06 s, as shown in Fig. 6b. The 0.06 s were selected to minimize the oscillations in the cable produced by ramping up the temperatures at lower values.

3.2.2. Post foundations

Building upon previous studies by Marzougui et al. [5], Bruski et al. [10], Bruski and Witkowski [18], Bruski et al. [3], and Wilde et al. [25,31], we used a computationally efficient approach to model the soil, by using individual solid cylinders near the impact location and equivalent spring elements far from the impact location, as shown in Fig. 5. Given that solid models are computationally intensive, the solid model was only used near the impact location —where accurate modeling of the interactions is needed— while

---

[3] As discussed later, a parametric analysis is conducted where this pretension load is varied to assess its effect on the performance of the cable barrier.
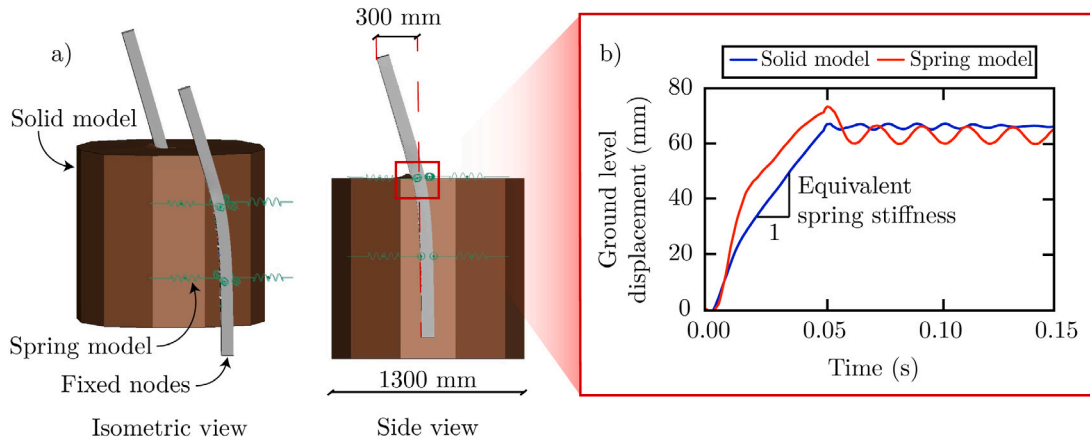
Fig. 7. Equivalent linear spring determination based on ground displacement.
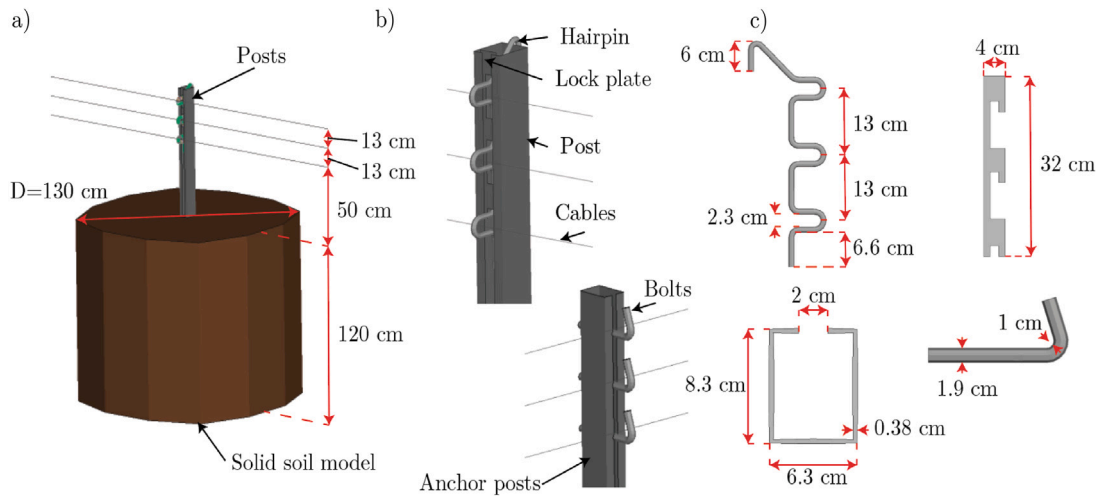

Fig. 8. Details of the posts and cable support system in guard cable barriers: (a) general view of the post-soil system, (b) components of the cable fastening mechanism, and (c) general dimensions of the hairpin, lock plate, post cross-section, and bolts. Two types of cable fastening systems are displayed: the typical system is composed of hairpins and lock plates, while the bolt fastening system is located only at the anchorages of the cable barrier.

the equivalent spring model was implemented far away from the impact location —where precise modeling of the interactions is not needed.

The solid cylinders were modeled using solid hexahedral elements with constant stress (ELFORM = 1) and the `MAT_005_SOIL_AND_FOAM` material model. The material density was 2200 kg/m^3, the bulk modulus was 75.43 GPa, and the shear modulus was 2.75 GPa. We used the hard soil yield function constants proposed by Klasztorny et al. [11], with a pressure cutoff for tensile fracture value of −0.3087. These parameters correspond to medium cohesive soils with intermediate stiffness typically found on roadsides [11].

To determine the equivalent linear stiffness of the simplified spring model, we applied a 300 mm lateral deformation at the top of the posts. We iteratively adjusted the spring stiffness until the ground displacement of the spring model matched that of the solid model, as shown in Fig. 7. Finally, we assigned the same `DAMPING_PART_STIFFNESS` card with a 10% damping coefficient recommended by Klasztorny et al. [11].

3.2.3. Hairpins and posts

We discretized the hairpin hooks as beam elements based on the Hughes–Liu formulation (ELFORM = 1) with material model `MAT_PIECEWISE_LINEAR_PLASTICITY` [3]. Additionally, we modeled the bolts (shown in Fig. 8) using fully-integrated solid elements (ELFORM = 2) [5,8]. Both the hairpin beams and bolts were covered with null shells (`MAT_NULL` material model, Belytschko–Tsay formulation, ELFORM = 2) to facilitate the contact modeling [8]. For the hairpin case, the null shells were kinematically constrained to the beam nodes using `NODAL_RIGID_BODY` (CNRB) entities, as shown in Fig. 3.

Table 3
Description of keywords implemented in the model.

Element	Description
Cables	Beam elements, Belytschko–Schwer resultant beam formulation (ELFORM = 2), MAT_MOMENT_CURVATURE_BEAM, material parameters from [7].
Tensioning elements	Beam elements, Hughes–Liu formulation (ELFORM = 1) with ELASTIC_PLASTIC_THERMAL, tensile force ranges between 16.8 and 28 kN.
Posts	Shell elements, Belytschko–Tsay formulation (ELFORM = 2) with MAT_PIECEWISE_LINEAR_PLASTICITY material model
Hairpins	Beam elements, Hughes–Liu formulation (ELFORM = 1) with material model MAT_PIECEWISE_LINEAR_PLASTICITY. Beam nodes kinematically constrained to shells elements of the MAT_NULL material model using Nodal Rigid Body (CNRB) constraints.
Bolts	Solid elements, fully-integrated formulation (ELFORM = 2) with MAT_PIECEWISE_LINEAR_PLASTICITY material model
Solid soil	Solid elements, constant stress formulation (ELFORM = 1). MAT_005_SOIL_AND_FOAM material model with parameters from [11].
Simplified soil	Discrete elements, SPRING_ELASTIC material model with stiffness calibrated to match the refined soil total deformation.
Contact	CONTACT_AUTOMATIC_GENERAL_INTERIOR for vehicle and cable barrier interaction, CONTACT_AUTOMATIC_SURFACE_TO_SURFACE for soil and post interaction, and CONTACT_INTERIOR for solid soil numerical stability
Damping	DAMPING_PART_STIFFNESS, for wire ropes, posts and solid soil, and DAMPING_FREQUENCY_RANGE for wire ropes only.

We modeled the post geometry using shell elements with a Belytschko–Tsay formulation (ELFORM = 2) and characteristic element dimensions of 0.3 × 0.3 cm. The elastoplastic properties of steel were modeled using the MAT_PIECEWISE_LINEAR_ PLASTICITY material model. The density was set to 7850 kg/m^3 and the Young's modulus to 205 GPa. Strain rate was accounted following the studies by Hallquist et al. [26] and Bruski et al. [3]. In their work, the Cowper and Symonds models is employed to scale the yield stress with the factor [26]

$$1 + \left(\frac{\dot{\epsilon}}{C}\right)^{\frac{1}{P}},$$

(1)

where $\dot{\epsilon}$ is the strain rate, and C and P are set to 8000 and 8 [3], respectively.

3.2.4. Contacts

We modeled the contact between the vehicle and the cables using the CONTACT_AUTOMATIC_GENERAL_INTERIOR keyword. We assigned a static coefficient of friction of 0.3 and a dynamic coefficient of friction of 0.2, corresponding to 2/3 of the static value [37]. The model includes the soft constraint formulation with a scale factor for constraint forces of 0.1 [5]. We also employed the contact type CONTACT_AUTOMATIC_GENERAL_INTERIOR to model the hairpin-to-post and the bolt-to-cable contacts. Additionally, we handled the remaining cable-to-post and the cable-to-bolts contacts using CONTACT_AUTOMATIC_GENERAL.

Soft materials that experience significant deformations, such as the foams utilized for simulating soil, may result in an element becoming distorted to the extent that its volume is computed as negative. To combat this issue, we assigned the internal contact CONTACT_INTERIOR card to the soil solids. This contact card removes elements that undergo extreme deformations and therefore prevents numerical instabilities resulting from negative volumes [3,11]. We handled the interaction between the soil and the posts using null shells at the interface and the contact algorithm CONTACT_AUTOMATIC_SURFACE_TO_SURFACE [3].

Table 3 presents a short description of the keywords implemented in the cable barrier model. Additionally, Table 4 provides some of the most important keyword parameters employed in the present study. All items included are described in detail in the Theory Documentation from LS-DYNA [26,38].

4. Validation

In this section, we validate the numerical model discussed previously by comparing our simulation results against experimental results from a full-scale crash test performed on a three-strand cable barrier [39]. Fig. 9 compares the vehicle trajectory obtained from our numerical model with observations from the full-scale crash tests reported by Gibraltar Cable Barrier Systems [39] at various time points. As can be seen from the figure, our numerical model captures the general kinematics of the physical test. First, the cable system effectively contains the vehicle, preventing it from entering opposing travel lanes. Then, the vehicle is redirected parallel to the cable barrier. It is worth noting that both the physical and the numerical tests display a cable deflection of around half the vehicle width. Finally, the vehicle is pushed back onto the correct travel lane with a relative lateral displacement between its rear- and front-ends, a behavior observed in both the physical and the numerical results.

Fig. 10a compares the evolving vehicle speed over time and the observed experimental speed data reported at the exit conditions. In the numerical model, the vehicle separates from the cable at 0.6 s with a speed of 70 km/h, which is 11% lower than the exit

Table 4

Material parameters used in the model. Units in ton, mm, s, N, and MPa.

Part	Material model	Parameter	Description	Value
Cables	MAT_MOMENT_CURVATURE_BEAM	RO	Mass density	4.309×10^{-9}
		E	Young's modulus	6.29×10^{4}
		CFA	Rigidities ratio	0.97
		REPS	Rupture effective axial strain	0.0185
Tensioning elements	ELASTIC_PLASTIC_THERMAL	RO	Mass density	4.309×10^{-9}
		E	Young's modulus	6.29×10^{4}
		ALPHA	Coefficient of thermal expansion	0.16
		T1,T2,T3	Temperatures at time 1,2 and 3	−1,0,1
Posts, bolts, hairpins and lock plate	PIECEWISE_LINEAR_PLASTICITY	RO	Mass density	7.85×10^{-9}
		E	Young's modulus	200×10^{5}
		C	Strain rate parameter	8000
		P	Strain rate parameter	8
Solid soil	MAT_005_SOIL_AND_FOAM	RO	Mass density	2.2×10^{-9}
		G	Shear modulus	2.75
		BULK	Bulk modulus	S: 32 H: 75.42
		A0	Yield function constant	S: 5.82×10^{-4} H: 2.5×10^{-2}
		A1	Yield function constant	S: 0.01 H: 0.03
		A2	Yield function constant	S: 0.04 H: 0.13
		PC	Pressure cutoff	S: -2 H: −0.3
Simplified soil	SPRING_ELASTIC	K	Elastic stiffness	Lower: 100 Upper: 75

speed reported experimentally. It is worth mentioning that guard cable collisions are complex dynamic problems, they are subjected to multiple physical constraints and site specific conditions that cannot be fully captured in a numerical model. Therefore, an 11% difference between the numerical and the experimental results is deemed acceptable.

The dynamic deflection of a cable barrier during an impact is a crucial characteristic of cable barriers because they have much greater deflections than semi-rigid W-beam barriers and rigid concrete barriers [23]. Therefore, in the event of large deflections, a vehicle could collide with rigid objects or, even worse, with a vehicle in the opposing traffic lane. Consequently, we used the dynamic deflection as a validation parameter in our study. Fig. 10b displays the change in cable deflection at the point of maximum deformation as a function of time and compares it with the maximum deflection reported in the physical test. We obtained a maximum cable deflection of 0.87 m, 15% higher than the value reported experimentally of 0.76 m. The difference between the numerical and the experimental results may stem from discrepancies in soil stiffness, impact angle, vehicle speed, or discrepancies in the total vehicle mass or front-end stiffness.

International standards such as EN 1317 [22] require evaluating the effects of the collision on vehicle occupants. One important parameter to consider is the acceleration severity index (ASI), which helps assess occupant injuries during impact and is computed as follows:

$$\text{ASI}(t) = \sqrt{\left(\frac{\bar{A}_x}{\hat{a}_x}\right)^2 + \left(\frac{\bar{A}_y}{\hat{a}_y}\right)^2 + \left(\frac{\bar{A}_z}{\hat{a}_z}\right)^2}, \tag{2}$$

where $\bar{A}_x$, $\bar{A}_y$, $\bar{A}_z$ represent, respectively, the acceleration along the longitudinal, lateral, and vertical directions at the vehicle center of gravity, and $\hat{a}_x = 12$ g, $\hat{a}_y = 9$ g, $\hat{a}_z = 10$ g are the limit values for the acceleration components. Fig. 10c shows the computed ASI as a function of time, where $\bar{A}_x$, $\bar{A}_y$, $\bar{A}_z$ were smoothened using a four-pole phaseless Butterworth low-pass digital filter with a cut-off frequency of 13 Hz [25]. During impact, a maximum ASI of 0.58 was obtained, corresponding to a 12% difference from the 0.66 value obtained experimentally [39]. These results provide an overall good comparison with the physical test and guarantee the reliability of the model in capturing the dynamic behavior of vehicular impacts.

5. Parametric study

Once the numerical model was validated, we performed a total of fourteen simulations to evaluate the performance of the cable barrier under different impact and system conditions. We conducted a comprehensive assessment to examine how various factors, including vehicle speed and impact angle (impact conditions), and cable pretension level and foundation material stiffness (system conditions), influence the resulting cable tensions and cable deflections during a vehicular impact. The different conditions
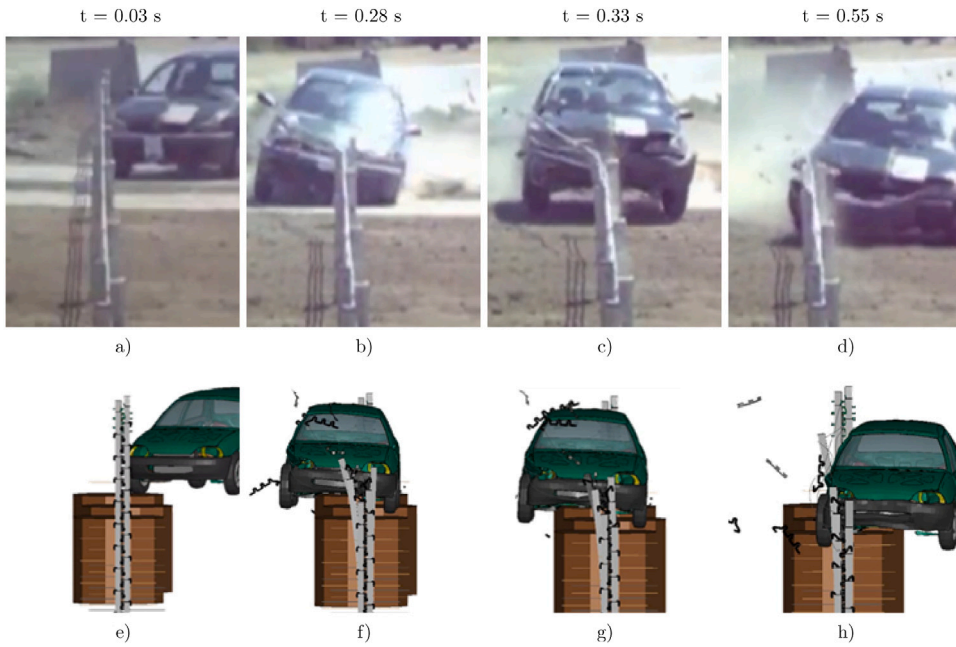
Fig. 9. Full-scale crash test and simulation comparisons: (a–d) Karco Engineering tests [39] and (e–h) numerical model results.
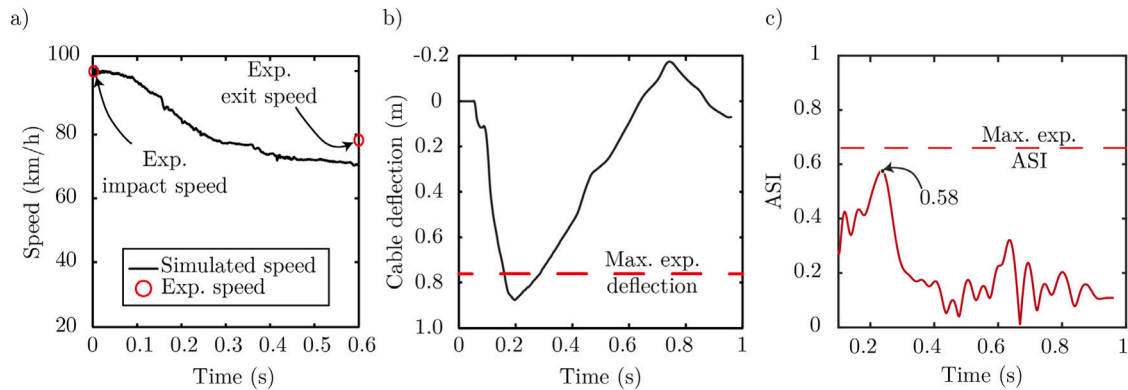

Fig. 10. Comparison between the results of the finite element model and the physical test: (a) vehicle speed during cable contact, (b) maximum cable deflection, and (c) maximum ASI.

considered in this parametric analysis are presented in Table 5. The hard and soft soil stiffness tags correspond to the soil models presented by Klasztorny et al. [11].

5.1. Influence of vehicle speed and impact angle

According to the National Cooperative Highway Research Program [2], the standard impact conditions for a 900 kg vehicle (test designation 820C) should be 20° as impact angle and 100 km/h for the vehicle speed. In this section, we analyze the performance of the cable barrier under different impact angles and speeds while keeping the pretension level constant at 28 kN and assuming a hard foundation soil (i.e., models S1–S9 from Table 5).

Fig. 11 displays the tension in the lower cable as a function of time and the maximum tension values, both at the impact location and at 90 m downstream, for different combinations of impact speed and angle. These results show that the tension in the cable increases at higher vehicle speeds and impact angles, as expected. As shown in Table 6, when the impact speed increases by 30 km/h and the impact angle by 20° relative to those for standard crash conditions, the maximum tension in the cable increases by up to 91%. Although the increased cable tension is not close to the cable tensile strength of 173.5 kN [7], it raises concerns about the ability of the cable barrier to contain heavier vehicles impacting at non-standard conditions. For instance, light trucks, which

Table 5

Impact conditions used for the parametric analysis.

Test	Vehicle speed (km/h)	Impact angle (°)	Pretension load (kN)	Foundation material stiffness
S1	100	20	28	Hard soil
S2	115	20	28	Hard soil
S3	130	20	28	Hard soil
S4	100	30	28	Hard soil
S5	115	30	28	Hard soil
S6	130	30	28	Hard soil
S7	100	40	28	Hard soil
S8	115	40	28	Hard soil
S9	130	40	28	Hard soil
S10	100	20	22.4	Hard soil
S11	100	20	19.6	Hard soil
S12	100	20	16.8	Hard soil
S13	100	20	28	Concrete
S14	100	20	28	Soft soil

Table 6

Maximum tensions and displacement in the lower cable under different combinations of non-standard impact conditions.

Case	Maximum tension (kN)				Maximum displacement (m)
	Impact location	Relative difference (%)	90 m downstream	Relative difference (%)	
$\theta = 20°$, $v = 100$ km/h[a]	56.7	–	51.5	–	1.2
$\theta = 20°$, $v = 115$ km/h	61.5	8.6	56.4	9.4	1.4
$\theta = 20°$, $v = 130$ km/h	63.8	12.5	63.8	23.8	1.6
$\theta = 30°$, $v = 100$ km/h	73.0	28.7	67.8	31.5	2.3
$\theta = 30°$, $v = 115$ km/h	84.7	49.4	74.0	43.5	2.6
$\theta = 30°$, $v = 130$ km/h	101.6	79.3	75.9	47.2	2.7
$\theta = 40°$, $v = 100$ km/h	93.9	67.5	85.8	66.4	3.2
$\theta = 40°$, $v = 115$ km/h	98.2	73.3	89.5	73.7	3.5
$\theta = 40°$, $v = 130$ km/h	108.4	91.3	99.0	92.0	4.0

[a] Values recommended by the National Cooperative Highway Research Program (NCHRP) report 350 [2].

comprise more than 60% of vehicles in operation in the United States [40] may not be effectively contained by a cable barrier if impacted at speeds and angles higher than those stipulated by NCHRP.

In Fig. 12, the cable deflection is shown for non-standard impact conditions. For the highest speed and impact angle case, the cable deflection increased by 318%, highlighting the increased risk of collisions with obstacles such as light posts, trees, or traffic signals. Additionally, there is a greater risk of head-on collisions with vehicles traveling in the opposite lane. The data indicates that vehicles at higher impact speeds require more time to be redirected by the cable barrier, resulting in a longer time occupying the opposite side of traffic and amplifying the risk of head-on collisions. As depicted in Fig. 13, our results show a linear relationship between maximum cable deflection and vehicle speed and impact angle, which agrees with findings reported by Fang et al. [17]. Moreover, from the comparison between Figs. 11 and 12, we can observe that the time of occurrence of the maximum forces corresponds to the time of the maximum cable deflections, confirming observations from Bruski et al. [20] on the performance of high-tension cable barriers installed on horizontal convex road curves.

In Fig. 14, we can observe the trajectories of the vehicle during tests S3, S6, and S9. It is evident from the figure that as the impact angle increases, the distance covered along the longitudinal direction of the barrier per second of simulation decreases. Nevertheless, a higher impact angle results in a greater lateral distance that the vehicle penetrates, consequently increasing the likelihood of head-on collisions.[4] Finally, from comparing the three trajectories, we can observe that larger impact angles produce more significant relative rotations between the vehicle rear-end and front-end, increasing the chances of the vehicle passenger side getting impacted by other cars traveling in the opposite direction.

Fig. 15 presents the ASIs obtained for the nine models. As shown, the values are always lower than one, corresponding to systems with the highest level of safety —level A [22]. These results are consistent with the elastic and *forgiving* nature of cable barriers [23] in which a lower impact severity is obtained through higher dynamic deflections when compared to rigid barriers such as W-beam guardrail barriers. Based on the figures, it is evident that there is no observable relationship between the severity of the impact at the passenger level and the impact angle or speed. These results suggest that, as the impact angle and speed increase, the severity of the collision at the passenger level remains below acceptable levels, and instead, the primary risk when hitting a guard cable is the potential for large cable deflections (cf., Fig. 12).

---

[4] The results for model S6 deviate from the general trend due to the cable becoming entangled with the car chassis. For this particular model, the cable got caught in the screen pillar of the vehicle, impeding it from returning to the travel lane at the same rate as the other models.
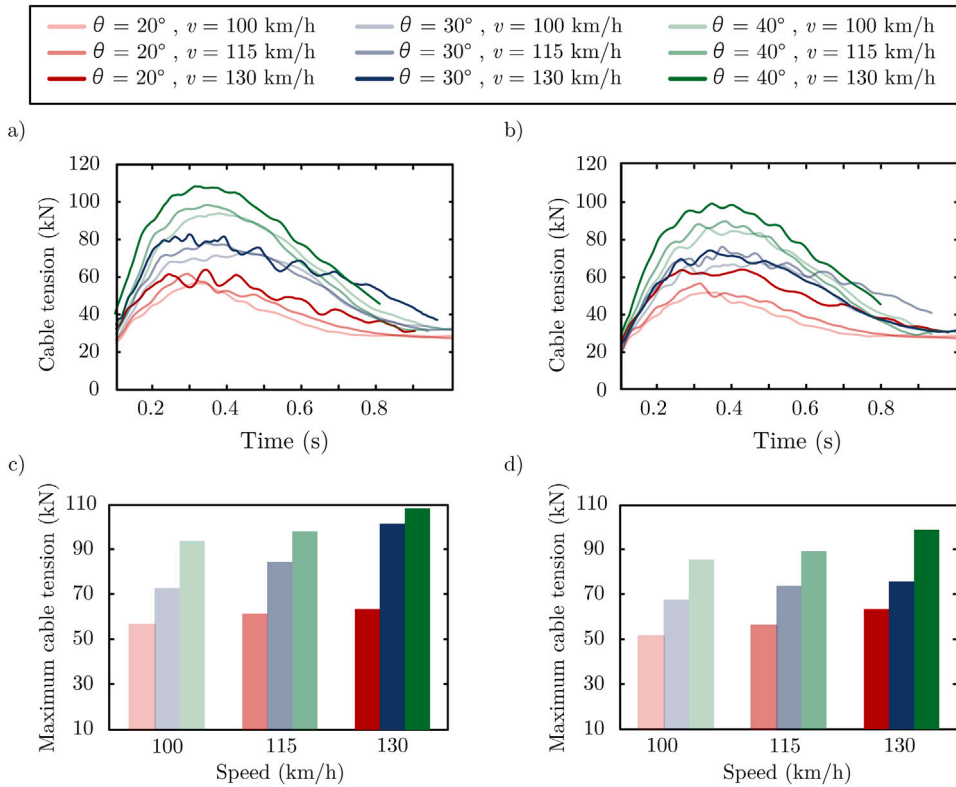
Fig. 11. Tension in the lower cable over time when impacted by a Chevrolet Geo Metro at impact location (a) and 90 m downstream (b) for different combinations of impact speed and impact angle. And maximum tension values at (c) impact location and (d) 90 m downstream.
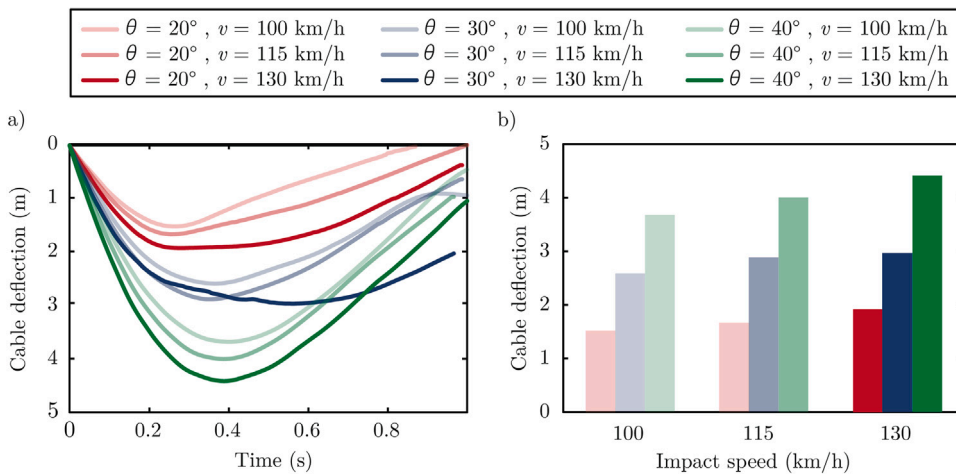

Fig. 12. Comparison of (a) cable deflection for different combinations of impact speed and impact angle and (b) maximum cable deflection for different combinations of impact speed and impact angle.

5.2. Influence of cable pretension

We performed four simulations to assess the influence of the cable pretension in the cable maximum tension and deflection during impact. In the first simulation (S1) we set the cable pretension as 28 kN (T_0). We then reduced the tension to 80%, 70% and 60% of T_0 (Tests S10, S11, and S12 respectively).

Fig. 16a presents the change in tension over time and its maximum values both at the impact location and at 90 m downstream. The figure shows no clear relationship between the pretension load and the maximum tension in the cable. However, the tension at
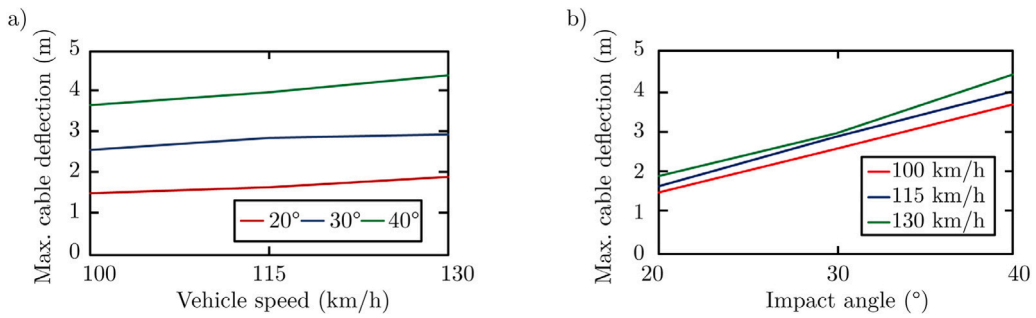
Fig. 13. Variation of the maximum cable deflection with respect to (a) the vehicle speed and (b) the impact angle.
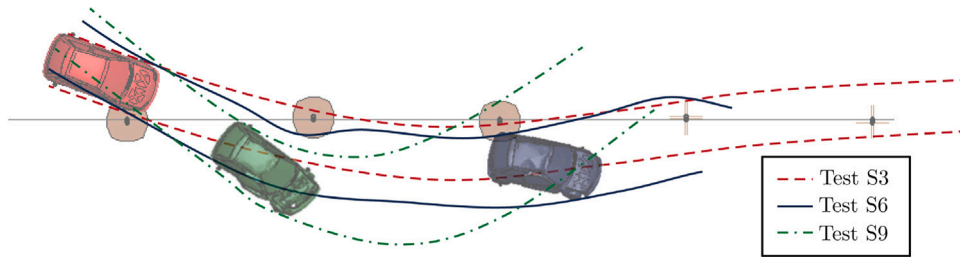

Fig. 14. Comparison of vehicle trajectory during tests S3, S6 and S9.
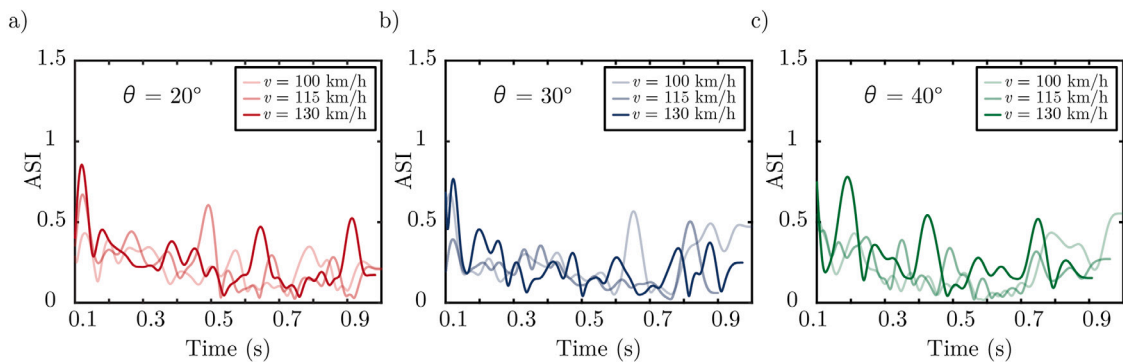

Fig. 15. Acceleration severity index (ASI) for different impact configurations: (a) 20° impact angle, (b) 30° impact angle and (c) 40° impact angle.

the impact location is generally 10% higher than that at 90 m downstream. This difference may be caused by localized stretching of the cable due to the relative deformation reduction caused by the posts and hairpins, as well as by energy dissipation due to friction between the cables and the hairpins/posts. Similar findings were reported by Reid et al. [27], who also observed changes in tension by adjusting the posts around which the cable is deflected. According to the authors, this change is due to an overall increase in cable strain caused by a steeper slope around the neighboring posts.

Fig. 17a depicts the cable deflection as a function of time and Fig. 17b shows the maximum cable deflection for various pretension levels. As it can be observed, lower levels of pretension produce higher transverse deformations. Particularly, a 40% reduction in the cable pretension leads to a 10% increase in the maximum cable deflection (compared to the fully tensioned system). The maximum deflection in the fully tensioned system occurs at around 0.25 s of simulation; under-tensioned systems exhibit their maximum deflection very close to this simulation time while also taking around the same time to return to the undeformed position.

5.3. Influence of foundation material stiffness

We created three numerical models, each for a different level of foundation material stiffness. The first model, which aims to simulate concrete foundations, was created by fixing the post nodes below the ground level. The second and third models considered foundations with intermediate and low stiffness values (see Table 4), which were created using the material parameters for hard and soft cohesive soils reported by Klasztorny et al. [11] and the available models from the NCAC repository [33]. In these soil models, harder soils presented higher values of shear modulus, bulk modulus, and higher yield strength [26].
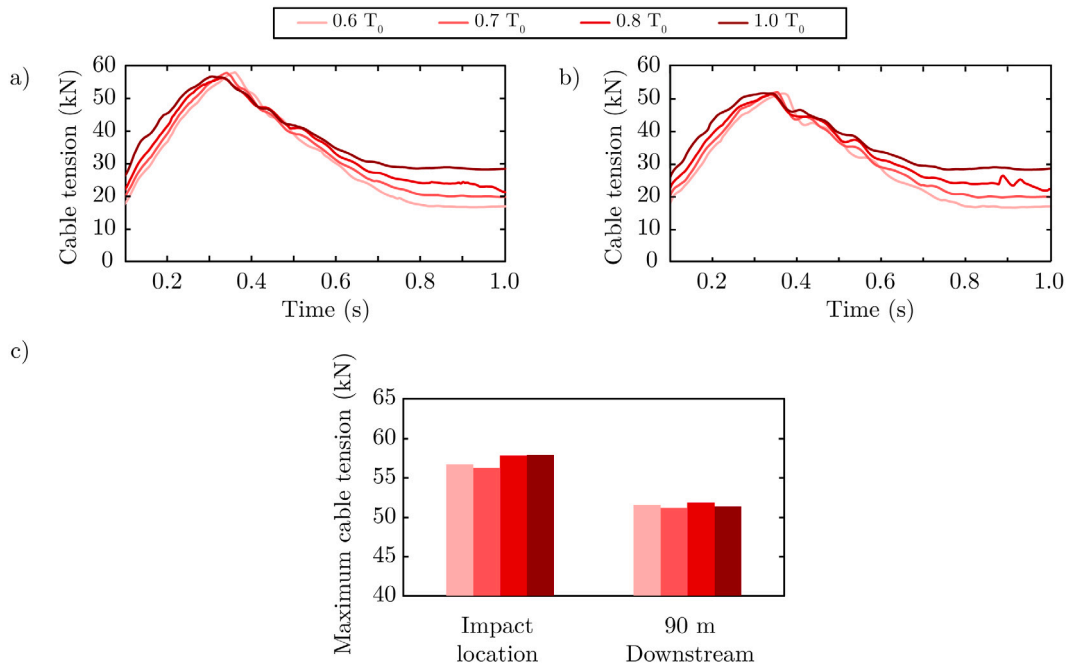
Fig. 16. Tension in the lower cable over time at (a) impact location and (b) 90 m downstream for different levels of pretension. And (c) maximum tension values for different levels of pretension at impact location and 90 m downstream.
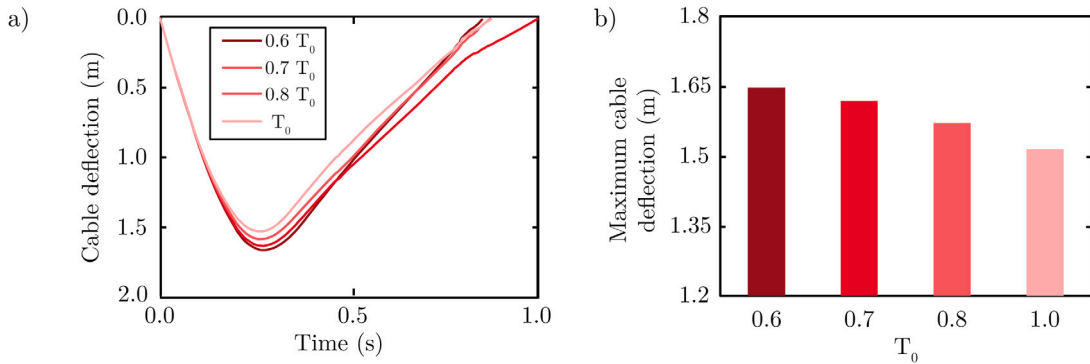

Fig. 17. Comparison of (a) cable deflection for different levels of pretension and (b) maximum deflection values for each level of pretension.

Fig. 18 presents the tension variation as a function of time both at the impact location (Fig. 18a) and at 90 m downstream (Fig. 18b) for different levels of foundation material stiffness. The maximum values of tension for each foundation material stiffness are presented in Fig. 18c. It is shown that stiffer materials lead to up to 13% higher tensions. Moreover, the difference in the maximum tension is more appreciable at the impact location. As observed in Fig. 18c, the difference in tensions between the stiffer and softer foundations is about 7.2 kN at the impact location; the difference goes down to 3.3 kN at 90 m downstream from the impact point. From comparing Figs. 18a and 19a, we can observe that although stiffer foundation materials produce larger tensions, this increment in the tension is accompanied by lower cable deflections (10% less). This effect is caused by the increased relative difference between the cable deflection at the impact point versus the deflection at 90 downstream. As discussed previously, this behavior results in a localized stretching of the cable (similar to the one mentioned in Section 5.2) in which lower absolute displacements result in higher cable tensions.

According to Fig. 19a, foundation materials with softer properties experience greater deflections and have a delayed peak deflection compared to stiffer materials. Additionally, cable barriers supported by softer foundations require a longer time to redirect a vehicle in the correct direction of travel. For example, cable barriers supported by hard soils take approximately 0.3 s longer to return to their original position (a cable deflection of zero) compared to those supported by concrete foundations. This difference is even more pronounced for soft soil cases, where the cable barrier takes twice as long as the concrete-supported ones to redirect a vehicle. This is concerning since the extended engagement between the soft soil-supported cable barriers and vehicles increases the likelihood of collisions and more significant damage to the barriers.
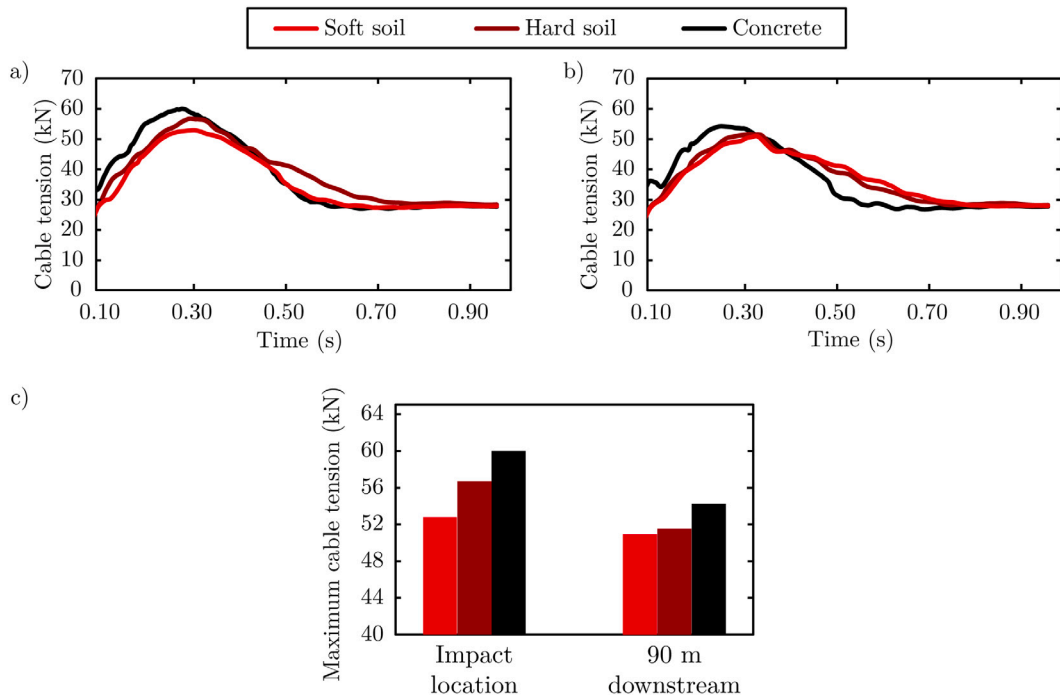
Fig. 18. Tension in the lower cable over time at (a) impact location and (b) at 90 m downstream for different levels of foundation material stiffness. And (c) maximum tension values at the impact location and 90 m downstream.
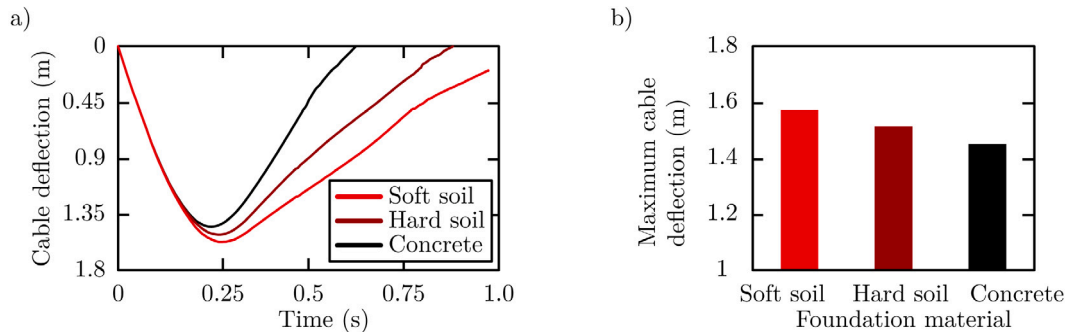

Fig. 19. Comparison of (a) cable deflection for different levels of foundation material stiffness, and (b) maximum displacement values for each level of foundation material stiffness.

6. Conclusions

In this study, we used LS-DYNA to develop a set of finite element models of a high-tension cable barrier to analyze its performance under various impact and system conditions. Our analysis focused on evaluating the performance of the cable barrier when impacted by a Chevrolet Geo Metro, while considering different impact conditions, such as impact speed and impact angle, as well as system conditions, including varying cable pretension loads and foundation material stiffness.

Overall, our findings suggest that evaluating parameters beyond those in standard safety manuals is crucial for assessing the effectiveness of cable barriers in real-world impact scenarios. Specifically, the results indicate that higher vehicle speeds and impact angles should be considered during roadside barrier certifications, as this approach provides a more comprehensive understanding of barrier performance under impact conditions typical of American highways. Additionally, our results highlight the importance of investigating the effects of construction features such as lower cable pretension loads and varying foundation material stiffness. These factors can significantly influence the behavior of cable barriers during vehicular impact and should be considered in performance evaluations. By extending the range of tested parameters, we can better understand the capabilities and limitations of cable barriers, ultimately leading to improved safety measures and more effective roadside barrier designs.

To validate the finite element models, we compared our simulation results under standard impact conditions (i.e., 100 km/h impact speed and 20° impact angle) against full-scale experimental test results conducted by a cable barrier manufacturer [39] and

available online. This critical validation step demonstrated the effectiveness of the model in capturing the intricate physical response of guard cables during impact events. The validation step showed that the finite element model successfully predicted the complex vehicle dynamics (such as vehicle position and orientation vs. time), vehicle speeds, cable barrier deflections, and safety parameters such as the acceleration severity index.

Once the model was validated, we conducted fourteen numerical simulations to evaluate cable tensions and cable lateral deflections. Nine of these simulations focused on different combinations of vehicle speed (100, 115, and 130 km/h) and impact angle (20°, 30°, and 40°). Additionally, we evaluated the effect of the pretension load in the cables and the relationship between the foundation material stiffness and barrier performance, considering four values of pretension load and three stiffness levels corresponding to soft soils, hard soils, and concrete.

Our findings showed that combinations of higher impact speeds and angles significantly increase cable tension and lateral deflection. For instance, an impact speed of 130 km/h and a 40° impact angle resulted in maximum cable tensions that were 91% higher than those under standard impact conditions. Similarly, these conditions also resulted in maximum cable deflections that were 318% higher than those observed under standard impact conditions. Based on these results, we conclude that speeding vehicles can cause significantly larger cable deflections, increasing the risk of head-on collisions or impacts with road obstacles such as light posts or traffic signals. Although the increased cable tensions did not exceed typical cable tensile strengths, larger vehicles could produce tensions that may exceed the strength limits. Given the traffic distribution on American highways, where light trucks comprise more than 60% of vehicles in operation [40], this issue warrants further investigation.

Our results also showed that as the impact angle increases, the distance covered along the longitudinal direction of the barrier decreases. Higher impact angles result in a greater cable deflections, ultimately increasing the chances of head-on collisions. Furthermore, our data revealed that higher impact angles produce more significant relative rotations between the rear end and front end of the vehicle, increasing the likelihood of the passenger side being impacted by other cars traveling in the opposite direction.

When evaluating the different system conditions, our results showed that softer foundation materials and under-tensioned systems lead to larger cable lateral deflections with lower tension variations. Under-tensioned cable barrier systems and those supported by softer foundations engage with the vehicle over larger distances than fully tensioned systems supported by stiff foundations, increasing the risk of hitting obstacles or impacting oncoming vehicles. Therefore, preventing soil degradation may help to avoid excessive barrier deflections, and thus, reduce the risk of head-on collisions or collisions with roadside obstacles. Interestingly, the cable deflections obtained from the various models show that increasing the cable pretension has a minimal effect on reducing cable deflections. This suggests that higher pretension forces may not significantly enhance the effectiveness of cable barriers. Conversely, factors such as impact speed and angle have the strongest effect on maximum cable forces and deflections during a collision, which suggests the need for further research focusing on these more influential factors to better understand and improve the design of cable barrier systems.

To summarize, numerical simulations using LS-DYNA allow to assess the performance of cable barrier systems with minimal cost as compared with real physical tests. The results from the numerical simulations provide unique insights that may assist road designers in identifying the most critical parameters affecting system performance, improving road safety systems, and and defining geometrical features such as clear zone widths in highways.

CRediT authorship contribution statement

Juan P. Giraldo-Isaza: Writing – original draft, Investigation. **Oliver Giraldo-Londoño:** Writing – review & editing, Validation, Supervision, Investigation. **Glenn A. Washer:** Writing – review & editing, Supervision, Investigation. **John J. Myers:** Writing – review & editing, Supervision, Investigation.

Declaration of competing interest

The authors declare that they have no known competing financial interests or personal relationships that could have appeared to influence the work reported in this paper.

Data availability

The authors do not have permission to share data.

Acknowledgments

References

[1] T.S.C. AAA Foundation for Traffic Safety, 2021 Traffic Safety Culture Index, Technical Report, 2022.
[2] H. Ross Jr., D. Sicking, R. Zimmer, National Cooperative Highway Research Program (NCHRP), Report 350: Recommended Procedures for the Safety Performance Evaluation of Highway Features, Technical Report, Tech. Rep., Transportation Research Board, National Research Council, 1993.
[3] D. Bruski, S. Burzyński, J. Chróścielewski, K. Jamroz, Ł. Pachocki, W. Witkowski, K. Wilde, Experimental and numerical analysis of the modified TB32 crash tests of the cable barrier system, Eng. Fail. Anal. 104 (2019) 227–246.
[4] P. Mohan, D. Marzougui, L. Meczkowski, N. Bedewi, Finite element modeling and validation of a 3-strand cable guardrail system, Int. J. Crashworthiness 10 (3) (2005) 267–273.
[5] D. Marzougui, P. Mohan, C.D. Kan, K. Opiela, Performance evaluation of low-tension three-strand cable median barriers, Transp. Res. Rec. 2025 (1) (2007) 34–44.
[6] E.L. Fasanella, K.H. Lyle, K.E. Jackson, Developing soil models for dynamic impact simulations, in: AHS International 65th Forum and Technology Display, 2009, Number LF99-7733.
[7] C.S. Stolle, J.D. Reid, Development of a wire rope model for cable guardrail simulation, Int. J. Crashworthiness 16 (3) (2011) 331–341.
[8] C.S. Stolle, J.D. Reid, R.W. Bielenberg, et al., Improved Models of Cable-to-Post Attachments for High-Tension Cable Barriers, Technical Report, Nebraska Transportation Center, 2012.
[9] S. Burzyński, J. Chróścielewski, Ł. Pachocki, Finite element method simulations of various cases of crash tests with N2/W4/A steel road barrier, in: MATEC Web of Conferences, Vol. 231, 2018, pp. 1–9.
[10] D. Bruski, S. Burzyński, J. Chróścielewski, Ł. Pachocki, K. Wilde, W. Witkowski, The influence of position of the post or its absence on the performance of the cable barrier system, in: MATEC Web of Conferences, Vol. 219, EDP Sciences, 2018, p. 02012.
[11] M. Klasztorny, D.B. Nycz, P. Dziewulski, R. Gieleta, M. Stankiewicz, K. Zielonka, Numerical modelling of post-ground subsystem in road safety barrier crash tests, Eng. Trans. 67 (4) (2019) 513–534.
[12] M. Miśkiewicz, D. Bruski, J. Chróścielewski, K. Wilde, Safety assessment of a concrete viaduct damaged by vehicle impact and an evaluation of the repair, Eng. Fail. Anal. 106 (2019) 104147.
[13] N. Dinnella, S. Chiappone, M. Guerrieri, The innovative "NDBA" concrete safety barrier able to withstand two subsequent TB81 crash tests, Eng. Fail. Anal. 115 (2020) 104660.
[14] H.I. Yumrutas, M.Y. Apak, Crashworthiness of the bollard system by experimentally validated virtual test, Eng. Fail. Anal. 148 (2023) 107167.
[15] N. Hiser, J. Reid, Modeling slip base mechanisms, Int. J. Crashworthiness 10 (5) (2005) 463–472.
[16] C.S. Stolle, J.D. Reid, Modeling wire rope used in cable barrier systems, in: Proceedings of the 11th International LS-DYNA Users Conference, 2010, pp. 1–10.
[17] H. Fang, Q. Wang, D.C. Weggel, Crash analysis and evaluation of cable median barriers on sloped medians using an efficient finite element model, Adv. Eng. Softw. 82 (2015) 1–13.
[18] D. Bruski, W. Witkowski, Numerical studies on the influence of selected construction features and road conditions on the performance of road cable barriers, in: MATEC Web of Conferences, Vol. 231, EDP Sciences, 2018, p. 01003.
[19] P. Baranowski, K. Damaziak, Numerical simulation of vehicle–lighting pole crash tests: Parametric study of factors influencing predicted occupant safety levels, Materials 14 (11) (2021) 2822.
[20] D. Bruski, S. Burzyński, W. Witkowski, Analysis of passenger car crash with a cable barrier installed with anti-glare screens on a horizontal convex road curve with 400 m radius, Int. J. Impact Eng. 173 (2023) 104486.
[21] PN-EN-1317-1, Road restraint systems. Part 1. Terminology and general criteria for test methods, 2010.
[22] PN-EN-1317-2, Road restraint systems. Part 2. Performance classes, impact test acceptance criteria and test methods for safety barriers including vehicle parapets, 2010.
[23] D. Marzougui, U. Mahadevaiah, F. Tahan, C.D.S. Kan, R. McGinnis, R. Powers, Guidance for the selection, use, and maintenance of cable barrier systems, Technical Report, Transportation Research Board, 2012.
[24] M.-G.K. Kee-Dong Kim, K.-J. Han, J.-W. Joo, Long-span semi-rigid cable barriers designed for high-impact severity satisfying the small car impact speed of 160 km/h, Int. J. Crashworthiness 25 (1) (2020) 54–73.
[25] K. Wilde, D. Bruski, M. Budzyński, S. Burzyński, J. Chróścielewski, K. Jamroz, Ł. Pachocki, W. Witkowski, Numerical analysis of TB32 crash tests for 4-cable guardrail barrier system installed on the horizontal convex curves of road, Int. J. Nonlinear Sci. Numer. Simul. 21 (1) (2020) 65–81.
[26] J.O. Hallquist, et al., LS-DYNA Theory Manual, Livermore Software Technology Corporation (LSTC), 2006.
[27] J.D. Reid, K.A. Lechtenberg, C.S. Stolle, Development of Advanced Finite Element Material Models for Cable Barrier Wire Rope, Technical Report, Nebraska Transportation Center, 2010.
[28] B.A. Lewis, et al., Manual for LS-DYNA Soil Material Model 147, Technical Report, United States. Federal Highway Administration, 2004.
[29] W. Wu, R. Thomson, A study of the interaction between a guardrail post and soil during quasi-static and dynamic loading, Int. J. Impact Eng. 34 (5) (2007) 883–898.
[30] D. Korczyk, Dynamic Analysis of Cubesat Impact on Lunar Surface Master's thesis, Embry-Riddle Aeronautical University, 2022.
[31] K. Wilde, D. Bruski, S. Burzyński, J. Chróścielewski, Ł. Pachocki, W. Witkowski, LS-DYNA simulations of the impacts of a 38-ton heavy goods vehicle into a road cable barrier, in: 12th European LS-DYNA Conference, 2019, pp. 20–22.
[32] L. Ying, X. Zhao, M. Dai, S. Zhang, P. Hu, Crashworthiness design of quenched boron steel thin-walled structures with functionally graded strength, Int. J. Impact Eng. 95 (2016) 72–88.
[33] K. Yonten, A. Eskandarian, Finite Element Model Archive, 2006, http://web.archive.org/web/20160408180243/http://www.ncac.gwu.edu/vml/models.html. (Visited 19 January 2023).
[34] M.R. Ferdous, A. Abu-Odeh, R.P. Bligh, H.L. Jones, N.M. Sheikh, Performance limit analysis for common roadside and median barriers using LS-DYNA, Int. J. Crashworthiness 16 (6) (2011) 691–706.
[35] D. Bruski, S. Burzyński, J. Chróścielewski, Ł. Pachocki, W. Witkowski, On the validation of the LS-DYNA geo metro numerical model, in: MATEC Web of Conferences, Vol. 262, EDP Sciences, 2019, p. 10001.
[36] KTC, Length of need — Highway Knowledge Portal — kp.uky.edu, 2023, https://kp.uky.edu/knowledge-portal/articles/length-of-need/#:~:text=Length%20of%20need%20(LON)%20represents,as%20excessive%20(AASHTO%202011). (Visited 20 June 2024).
[37] J.D. Reid, N. Hiser, Friction modelling between solid elements, Int. J. Crashworthiness 9 (1) (2004) 65–72.
[38] J. Hallquist, LS-DYNA Keyword User's Manual, Livermore Software Technology Corporation (LSTC), 2012.
[39] G.G. Gibraltar Cable Barrier Systems, Highway cable barrier system TL-3 - NCHRP report 350, 2005, https://gibraltarglobal.com/products/tl-3/. (Visited 19 January 2023).
[40] A. Hula, A. Maguire, A. Bunker, T. Rojeck, S. Harrison, The 2022 EPA Automotive Trends Report: Greenhouse Gas Emissions, Fuel Economy, and Technology Since 1975, Technical Report, United States Environmental Protection Agency, 2022.